J|A|C|S ARTICLES

Published on Web 10/21/2010

Intricate Role of Water in Proton Transport through Cytochrome *c* Oxidase

Hyun Ju Lee,[†,‡] Emelie Svahn,[†,‡] Jessica M. J. Swanson,[‡,§] Håkan Lepp,[†,||] Gregory A. Voth,[§,⊥] Peter Brzezinski,[*,†] and Robert B. Gennis[#]

Department of Biochemistry and Biophysics, The Arrhenius Laboratories for Natural Sciences, Stockholm University, SE-106 91 Stockholm, Sweden, Department of Chemistry, James Franck Institute, and Computation Institute, University of Chicago, 5735 South Ellis Avenue, Chicago, Illinois 60637, United States, and Department of Biochemistry, University of Illinois, Urbana, Illinois 61801, United States

Received August 12, 2010; E-mail: peterb@dbb.su.se

Abstract: Cytochrome *c* oxidase (Cyt*c*O), the final electron acceptor in the respiratory chain, catalyzes the reduction of O_2 to H_2O while simultaneously pumping protons across the inner mitochondrial or bacterial membrane to maintain a transmembrane electrochemical gradient that drives, for example, ATP synthesis. In this work mutations that were predicted to alter proton translocation and enzyme activity in preliminary computational studies are characterized with extensive experimental and computational analysis. The mutations were introduced in the D pathway, one of two proton-uptake pathways, in Cyt*c*O from *Rhodobacter sphaeroides*. Serine residues 200 and 201, which are hydrogen-bonded to crystallographically resolved water molecules halfway up the D pathway, were replaced by more bulky hydrophobic residues (Ser200Ile, Ser200Val/Ser201Val, and Ser200Val/Ser201Tyr) to query the effects of changing the local structure on enzyme activity as well as proton uptake, release, and intermediate transitions. In addition, the effects of these mutations on internal proton transfer were investigated by blocking proton uptake at the pathway entrance (Asp132Asn replacement in addition to the above-mentioned mutations). Even though the overall activities of all mutant Cyt*c*O's were lowered, both the Ser200Ile and Ser200Val/Ser201Val variants maintained the ability to pump protons. The lowered activities were shown to be due to slowed oxidation kinetics during the $P_R \rightarrow F$ and $F \rightarrow O$ transitions (P_R is the "peroxy" intermediate formed at the catalytic site upon reaction of the four-electron-reduced Cyt*c*O with O_2, F is the oxoferryl intermediate, and O is the fully oxidized Cyt*c*O). Furthermore, the $P_R \rightarrow F$ transition is shown to be essentially pH independent up to pH 12 (i.e., the apparent pK_a of Glu286 is increased from 9.4 by at least 3 pK_a units) in the Ser200Val/Ser201Val mutant. Explicit simulations of proton transport in the mutated enzymes revealed that the solvation dynamics can cause intriguing energetic consequences and hence provide mechanistic insights that would never be detected in static structures or simulations of the system with fixed protonation states (i.e., lacking explicit proton transport). The results are discussed in terms of the proton-pumping mechanism of Cyt*c*O.

1. Introduction

Complex four in the respiratory chain, cytochrome *c* oxidase (Cyt*c*O), catalyzes oxidation of cytochrome *c* and the reduction of dioxygen to water. In cytochrome aa_3 (Cyt*c*O having two *a*-type hemes) from *Rhodobacter sphaeroides*, electrons are initially transferred one-by-one to a copper center, Cu_A, which is located near the cytochrome *c* binding site on the positive (P) side of the membrane. From Cu_A the electrons are transferred consecutively to a heme group (heme *a*) and then to the catalytic site, which consists of a copper site (Cu_B) and another heme group (heme a_3) in close proximity. Each electron transfer from cytochrome *c* to the catalytic site is linked to the uptake of one proton, from the negative (N) side of the membrane, which is used in the O_2 reduction reaction. Furthermore, each electron transfer to the catalytic site is linked to pumping of one proton across the membrane. Thus, for each O_2 reduced to H_2O a total of eight protons are taken up from the N-side of the membrane and four protons are released to the P-side:

$$4c_P^{2+} + O_2 + 8H_N^{+} \rightarrow 2H_2O + 4c_P^{3+} + 4H_P^{+}$$

where $c^{2+/3+}$ is reduced and oxidized cytochrome *c*, respectively, and the subscripts "N" and "P" indicate the N- and P-sides of the membrane. The proton electrochemical gradient that is generated by Cyt*c*O and other respiratory complexes is used, for example, to drive ATP synthesis by the ATPase.

Crystal structures of Cyt*c*O's and mutagenesis studies revealed two proton-uptake pathways in bacterial aa_3-type Cyt*c*O's: the D and K pathways. For each O_2 that is reduced to water, the K pathway is used to transfer one or two protons

[†] Stockholm University.
[§] Computation Institute, University of Chicago.
[⊥] Department of Chemistry, James Franck Institute, University of Chicago.
[#] University of Illinois.
[‡] These authors contributed equally.
[||] Current address: Experimental Biomolecular Physics, Department of Applied Physics, Royal Institute of Technology, Albanova University Center, SE-106 91 Stockholm, Sweden.

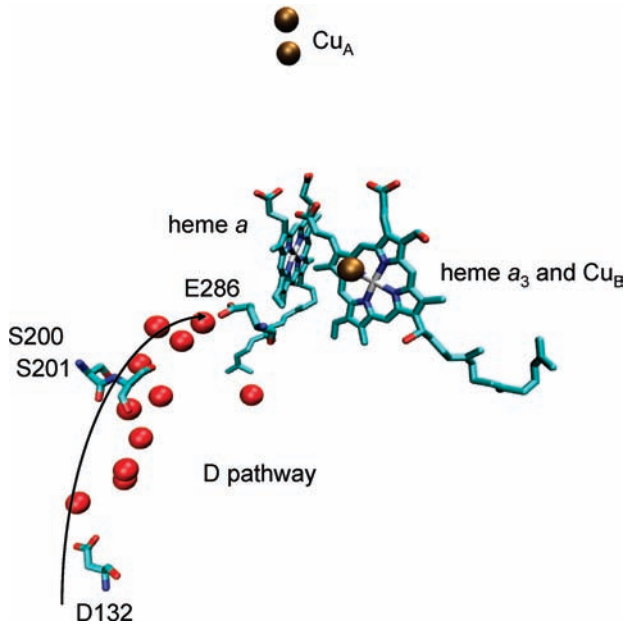

Figure 1. D pathway in Cyt*c*O. The pathway starts near D132 and leads to E286 via a number of water molecules that are resolved in the X-ray crystal structures.

upon initial electron transfer to the catalytic site, while the D pathway is used to transfer the remaining six to seven protons (i.e., at least two protons that are used for O_2 reduction and all four protons that are pumped). The D pathway (Figure 1) starts near Asp132 (D132) on the N-side of the membrane and leads to Glu286 (E286) via approximately 10−12 water molecules, 10 of which have been resolved in the X-ray crystal structures (12 water molecules have been suggested on the basis of simulation[1]). Glutamic acid 286 is buried about halfway into the membrane-spanning part of the protein. Protons are transferred from E286 to either the catalytic site or an acceptor site of pumped protons, which is located above the catalytic site closer to the P-side of the membrane (for recent reviews on the structure and function of Cyt*c*O's, see refs 2−9).

Because the D pathway is used to transfer both substrate protons and protons that are pumped across the membrane, the mechanism of proton transfer through this pathway has attracted much interest. As indicated above, E286 has been implicated as the branching point from which the trajectories from substrate and pumped protons lead in different directions.[10] In addition, the water molecules around E286 and in the D pathway are thought to influence the proton-transfer kinetics and the apparent pK_a of the residue (for a review, see ref 11). These water molecules are stabilized by hydrogen bonds with conserved residues in the D pathway. Replacement of some of these residues, using site-directed mutagenesis, has resulted in uncoupling of proton pumping from the oxygen reduction (i.e., these "uncoupled mutants" have partially or completely blocked proton pumping but maintain enzyme activity). There are two categories of such uncoupled mutants (reviewed in refs 3, 11, and 12): (i) those in which proton transfer through the D pathway is slowed[13] and (ii) those in which the proton-transfer kinetics is not altered or is slowed only to a small degree.[14−21] In the first case, the uncoupling might be explained by the slowed proton transfer because proton pumping most likely requires rapid protonation of a "pumping site" (when comparing the rate to that of electron transfer and proton transfer to the catalytic site). In the second case, the uncoupling must be due to specific modifications of components of the proton-pumping machinery. One illustrative example of category *ii* is the Asn139Asp (N139D) mutant Cyt*c*O in which proton transfer to the catalytic site is the same (or even slightly faster) as that in wild-type (WT) Cyt*c*O, but proton pumping is completely impaired.[17] The only other measurable alteration as a result of the N139D mutation was an increase in the E286 pK_a from 9.4 in the wild type to ∼11 in the mutant. The reason for the elevated pK_a is not known, but one possibility is altered solvation in the D pathway.[22,23] The reasons for uncoupling have also been postulated on the basis of theoretical calculations.[1,24,25] Results from another study showed that replacement of Ser197 (S197), which is hydrogen bonded to water molecules close to E286 (∼7 Å below), by Ala did not result in any changes in function, which indicates that there is some degree of plasticity in the water coordination of the D pathway.[20] Replacement of the same residue by Asp resulted in a lower overall activity, uncoupling of proton pumping from O_2 reduction, and a change in the pH dependence of the proton-transfer rate.[20] Additionally, early studies of a Ser201Ala (S200A) mutant showed that it

(1) Henry, R. M.; Yu, C. H.; Rodinger, T.; Pomès, R. *J. Mol. Biol.* **2009**, *387*, 1165.
(2) Gennis, R. B. *Front. Biosci.* **2004**, *9*, 581.
(3) Brzezinski, P.; Gennis, R. B. *J. Bioenerg. Biomembr.* **2008**, *40*, 521.
(4) Brändén, G.; Gennis, R. B.; Brzezinski, P. *Biochim. Biophys. Acta* **2006**, *1757*, 1052.
(5) Brzezinski, P.; Ädelroth, P. *Curr. Opin. Struct. Biol.* **2006**, *16*, 465.
(6) Wikström, M.; Verkhovsky, M. I. *Biochim. Biophys. Acta, Bioenerg.* **2007**, *1767*, 1200.
(7) Wikström, M.; Verkhovsky, M. I. *Biochim. Biophys. Acta, Bioenerg.* **2006**, *1757*, 1047.
(8) Hosler, J. P.; Ferguson-Miller, S.; Mills, D. A. *Annu. Rev. Biochem.* **2006**, *75*, 165.
(9) Brunori, M.; Giuffre, A.; Sarti, P. *J. Inorg. Biochem.* **2005**, *99*, 324.
(10) Iwata, S.; Ostermeier, C.; Ludwig, B.; Michel, H. *Nature* **1995**, *376*, 660.
(11) Brzezinski, P.; Johansson, A. L. *Biochim. Biophys. Acta, Bioenerg.* **2010**, *1797*, 710.
(12) Namslauer, A.; Brzezinski, P. *FEBS Lett.* **2004**, *567*, 103.
(13) Fetter, J. R.; Qian, J.; Shapleigh, J.; Thomas, J. W.; García-Horsman, A.; Schmidt, E.; Hosler, J.; Babcock, G. T.; Gennis, R. B.; Ferguson-Miller, S. *Proc. Natl. Acad. Sci. U.S.A.* **1995**, *92*, 1604.
(14) Pfitzner, U.; Hoffmeier, K.; Harrenga, A.; Kannt, A.; Michel, H.; Bamberg, E.; Richter, O. M. H.; Ludwig, B. *Biochemistry* **2000**, *39*, 6756.
(15) Pawate, A. S.; Morgan, J.; Namslauer, A.; Mills, D.; Brzezinski, P.; Ferguson-Miller, S.; Gennis, R. B. *Biochemistry* **2002**, *41*, 13417.
(16) Han, D.; Namslauer, A.; Pawate, A.; Morgan, J. E.; Nagy, S.; Vakkasoglu, A. S.; Brzezinski, P.; Gennis, R. B. *Biochemistry* **2006**, *45*, 14064.
(17) Namslauer, A.; Pawate, A. S.; Gennis, R. B.; Brzezinski, P. *Proc. Natl. Acad. Sci. U.S.A.* **2003**, *100*, 15543.
(18) Siletsky, S. A.; Pawate, A. S.; Weiss, K.; Gennis, R. B.; Konstantinov, A. A. *J. Biol. Chem.* **2004**, *279*, 52558.
(19) Lepp, H.; Salomonsson, L.; Zhu, J. P.; Gennis, R. B.; Brzezinski, P. *Biochim. Biophys. Acta* **2008**, *1777*, 897.
(20) Namslauer, A.; Lepp, H.; Brändén, M.; Jasaitis, A.; Verkhovsky, M. I.; Brzezinski, P. *J. Biol. Chem.* **2007**, *282*, 15148.
(21) Brändén, G.; Pawate, A. S.; Gennis, R. B.; Brzezinski, P. *Proc. Natl. Acad. Sci. U.S.A.* **2006**, *103*, 317.
(22) Vakkasoglu, A. S.; Morgan, J. E.; Han, D.; Pawate, A. S.; Gennis, R. B. *FEBS Lett.* **2006**, *580*, 4613.
(23) Duerr, K. L.; Koepke, J.; Hellwig, P.; Mueller, H.; Angerer, H.; Peng, G.; Olkhova, E.; Richter, O. M. H.; Ludwig, B.; Michel, H. *J. Mol. Biol.* **2008**, *384*, 865.
(24) Olsson, M. H.; Warshel, A. *Proc. Natl. Acad. Sci. U.S.A.* **2006**, *103*, 6500.
(25) Xu, J.; Voth, G. A. *Biochim. Biophys. Acta* **2006**, *1757*, 852.

Table 1. Comparison of the Enzyme Activities of the Controlled and Uncontrolled States, Respiratory Control Ratios (RCR), and Proton-Pumping Efficiencies of WT and Mutant Oxidases from *R. sphaeroides*

	activity, $e^- s^{-1}$ (cytochrome aa_3)$^{-1}$				
Cyt*c*O	solublized Cyt*c*O (percentage of the WT value)	vesicles (controlled)	vesicles (uncontrolled)	RCR	proton-pumping efficiency, H^+/e^- (percentage of the WT value)
WT	1100 (100)	32	310	10	0.5 (100)
S200I	910 (83)	12	890	8.1	0.42 (85)
S200V/S201V	410 (37)	53	150	2.5	0.23 (46)
S200V/S201Y	120 (11)	26	65	2.8	0
D132N/S200I	32 (2.9)	83	15	0.2	0
D132N/S200V/S200V	73 (6.7)	92	39	0.3	0
D132N/S200V/S201Y	72 (6.5)	65	39	0.4	0

displays 50% activity compared to that of the wild-type Cyt*c*O, but maintains unaffected proton-pumping stoichiometry.[26]

Collectively, these results indicate that understanding the design of the proton-pumping machinery of Cyt*c*O requires understanding the detailed interactions between amino acid residues, water molecules, and the excess proton within the D pathway. A region that is of particular interest in this respect is a water cluster near two serine residues, Ser200 (S200) and Ser201 (S201). This cluster has been postulated to define a "proton trapping" region ~7 Å below E286 on the basis of an ~18 kcal/mol minimum that was revealed by explicit proton transport simulations of the mitochondrial Cyt*c*O with E286 in its protonated state.[25,27,28] The existence of a protonated water cluster was further supported by a crystal structure of the oxidized *R. sphaeroides* Cyt*c*O (PDB ID 2GSM) in which water oxygen atoms were resolved in closer proximity than the typical water hydrogen bond.[29]

To further challenge the existence of a "trapped proton" in the D pathway, preliminary proton transport simulations were carried out on a variety of mutations thought likely to disrupt the local solvation structure without introducing altered protonation states. On the basis of these simulations, three mutations were proposed for further investigation: Ser200Ile (S200I), Ser200Val/Ser201Val (S200V/S201V), and Ser200Val/Ser201Tyr (S200V/S201Y). In this study, we present the experimental and theoretical results of these investigations as well as the experimental characterization of internal proton transfer in enzymes with an additional mutation, Asp132Asn (D132N), which blocks proton uptake from solution near the N-side surface of the protein. The data show that the S200I, S200V/S201V, and S200V/S201Y structural modifications result in lower catalytic activities, but only S200V/S201Y completely impairs proton pumping. Additionally, the apparent pK_a of E286 is elevated from 9.4 in the wild-type Cyt*c*O to >12 in the S200V/S201V mutant. The theoretical results show that proton transport through the "trap region" is indeed altered in the mutated enzymes. When E286 is protonated (neutral), the S200V/S201V mutation introduces a barrier to proton transport, low in the trap region, while S200V/S201Y presents a larger barrier higher in the pathway, closer to E286. However, when E286 is deprotonated, neither mutant introduces a barrier in the pathway. Rather, proton transport to the negatively charged glutamic acid is a downhill process in the mutants, just as it is in the wild-type enzyme.[25,27]

The addition of the D132N mutation to the above-mentioned mutant Cyt*c*O's does not change the kinetics for the first measured transition ($P_R \rightarrow F$) (P_R is the "peroxy" intermediate formed at the catalytic site upon reaction of the four-electron-reduced Cyt*c*O with O_2, and F is the oxoferryl intermediate) in the wild-type or the mutated enzymes, indicating that this transition is not rate-limited by proton transport through the D pathway. The theoretical results suggest that the second transition ($F \rightarrow O$) (O is the fully oxidized Cyt*c*O) is also not rate-limited by proton transport through the D pathway since the mutations slow this transition significantly, but do not introduce a barrier in the free energy profiles of proton transport to the deprotonated form of E286. The simulations also reveal changes in the solvation structure within the D pathway that are both more complicated and more subtle than was anticipated on the basis of the experimental findings. Collectively, the results show that the dynamical details of the water in the D pathway are important for maintaining rapid proton-transfer rates and functional proton pumping.

2. Results

2.1. Steady-State Activities. All of the investigated mutants displayed lower steady-state activities compared to the wild-type Cyt*c*O (see Table 1). Removing a single hydroxyl group in the S200I mutant resulted in a relatively high steady-state activity (83% of the wild-type value). The S200V/S201V mutation decreased the steady-state activity to 37% of that of the wild-type Cyt*c*O, while introduction of a Tyr residue at position 201 (S200V/S201Y) resulted in a further decrease in the activity (11% of the wild-type Cyt*c*O value).

2.2. Respiratory Control and Proton Pumping. To determine the proton-pumping stoichiometries, the mutant Cyt*c*O's were reconstituted in lipid vesicles. First, the respiratory control ratios (RCRs), defined as the ratio of uncontrolled (i.e., with the H^+ and K^+ ionophores (CCCP and valinomycin) added to the vesicles) and controlled (with only valinomycin added) activities were determined to verify that the Cyt*c*O-containing vesicles were tight (i.e., not leaking protons). The mutant Cyt*c*O's displayed RCRs > 2 (see Table 1, where an RCR of >1 is indicative of an intact membrane). As observed previously[13,30] structural variants of Cyt*c*O's carrying the Asp132Asn (D132N) mutation displayed reversed RCRs (<1), indicating that protons could be provided from the (wrong) positive side of the membrane.

(26) Mitchell, D. M.; Fetter, J. R.; Mills, D. A.; Ädelroth, P.; Pressler, M. A.; Kim, Y.; Aasa, R.; Brzezinski, P.; Malmström, B. G.; Alben, J. O.; Babcock, G. T.; Ferguson-Miller, S.; Gennis, R. B. *Biochemistry* **1996**, *35*, 13089.
(27) Xu, J.; Voth, G. A. *Proc. Natl. Acad. Sci. U.S.A.* **2005**, *102*, 6795.
(28) Xu, J.; Sharpe, M. A.; Qin, L.; Ferguson-Miller, S.; Voth, G. A. *J. Am. Chem. Soc.* **2007**, *129*, 2910.
(29) Qin, L.; Hiser, C.; Mulichak, A.; Garavito, R. M.; Ferguson-Miller, S. *Proc. Natl. Acad. Sci. U.S.A.* **2006**, *103*, 16117.
(30) Mills, D. A.; Ferguson-Miller, S. *Biochim. Biophys. Acta, Bioenerg.* **1998**, *1365*, 46.

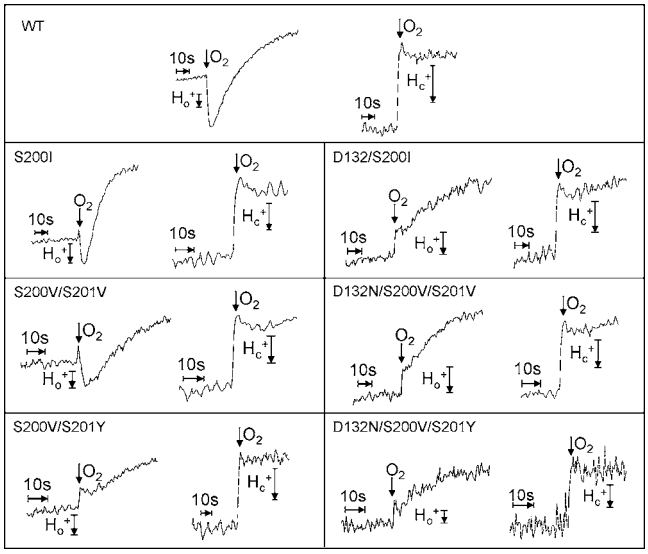

Figure 2. Results from proton-pumping measurements with the wild-type and mutant Cyt*c*O's (as indicated in the boxes) reconstituted in vesicles. Without CCCP (proton ionophore) the proton pumping leads to an acidification on the outside of the vesicles (H_O^+). Upon addition of CCCP the net uptake of protons by Cyt*c*O results in an alkalization upon initiation of the reaction (H_C^+). The H_O^+ and H_C^+ bars indicate a ΔpH of 0.001.

Proton pumping was measured by monitoring pH changes outside the vesicles after addition of a small amount of O_2 to the anaerobic vesicle−Cyt*c*O solution using a pH-sensitive electrode. With the wild-type Cyt*c*O a rapid acidification of the external medium, due to proton release, was observed. It was followed by a slow alkalization of the medium owing to proton leakage back into the vesicles. In the presence of the proton ionophore CCCP, alkalinization was detected due to the consumption of protons during the oxygen reduction. This signal was used to normalize the proton-pumping stoichiometry as (for a given amount of O_2) the total signal corresponds to one proton consumed per electron transferred to O_2. The results from the proton-pumping measurements are shown in Figure 2, and the stoichiometries are given in Table 1.

The S200I mutant Cyt*c*O pumped protons with almost the same stoichiometry as the wild-type Cyt*c*O. The S200V/S201V double-mutant Cyt*c*O displayed a proton pumping efficiency that was 46% of that of the wild-type Cyt*c*O, while the S200V/S201Y double mutant did not pump protons. Furthermore, the addition of the D132N mutation in all of the studied mutants resulted in impaired proton pumping (the D132N single mutant does not pump protons[13]).

The proton-pumping measurements were also repeated using a different assay based on the use of a pH-sensitive dye to monitor proton release (not shown). These studies gave the same results as those described above.

2.3. Oxidation and Reduction Kinetics. To determine the reduction kinetics, the fully oxidized enzyme was mixed with a solution containing ruthenium(III) hexamine (reducing agent) in a stopped-flow apparatus, after which absorbance changes were monitored at 445 nm. The oxidation kinetics was monitored at the same wavelength after the reduced enzyme was mixed with an O_2-containing solution in a stopped-flow apparatus. For the S200I mutant the decrease in the oxidation rate (53% of that obtained with the wild-type Cyt*c*O) was larger than that of the reduction rate (87%). The small decrease in these rates is consistent with the small decrease in the overall activity of this mutant. As shown in Table 2 both the reduction and oxidation rates of the S200V/S201V and S200V/S201Y double mutants were slowed. However, the oxidation rates were slowed to a much larger degree than the reduction rates, indicating that the decreased overall activities of these mutated Cyt*c*O's were due to the slowed oxidative part of the reaction.

Table 2. Oxidation and Reduction Rate Constants of WT and Mutant Cyt*c*O's[a]

Cyt*c*O	reduction rate constant (s^{-1}) (percentage of the WT value)	oxidation rate constant (s^{-1}) (percentage of the WT value)	$P_R \rightarrow F$ rate constant (s^{-1})	$F \rightarrow O$ rate constant (s^{-1})
WT	280	626	10000	500−1000
S200I	240 (87)	330 (53)	nd	nd
S200V/S201V	180 (63)	26 (4)	130	34
S200V/S201Y	280 (100)	2 (0.3)	70	5
D132N/S200I	330/280 (100)	3 (0.5)	nd	nd
D132N/S200V/S201V	260 (93)	15 (2)	200	5
D132N/S200V/S201Y	44 (16)	6 (1)	nd	nd

[a] nd = not determined.

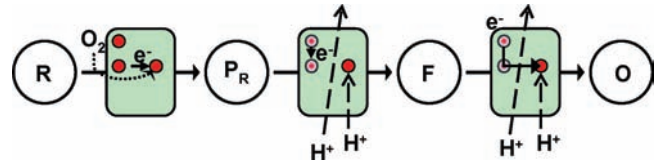

Figure 3. Schematic illustration of the reaction of reduced Cyt*c*O with O_2. The one-letter codes indicate the states of the Cyt*c*O: R, reduced state; P_R, peroxy state; F, ferryl state; O, oxidized state. During the $R \rightarrow P_R$ reaction, O_2 binds to heme a_3, an electron is transferred to the catalytic site from heme *a*, and the O−O bond is broken. During the $P_R \rightarrow F$ reaction, one proton is transferred to the catalytic site, one proton is pumped, and the electron at Cu_A equilibrates with heme *a*. Finally, during the $F \rightarrow O$ reaction, the electron in the heme a−Cu_A equilibrium is transferred to the catalytic site, a proton is taken up from solution, and a proton is pumped.

2.4. Flow-Flash Kinetics: Optical Detection. To determine rates of internal proton-transfer reactions and transitions between specific intermediate states that are formed during oxidation of the reduced Cyt*c*O, we investigated this reaction using the flow-flash technique.

Before we discuss the results for the mutated Cyt*c*O's, we briefly summarize results from earlier studies of the wild-type Cyt*c*O (see Figures 3 and 4A). The $P_R \rightarrow F$ transition, which involves proton uptake through the D pathway, is seen as an increase in absorbance at 580 nm with a time constant of ~100 μs at pH 7.4 (time constants are given as the inverse of the rate constants). It is followed by a decrease in absorbance with a time constant of ~1 ms, associated with the $F \rightarrow O$ transition, which involves electron and proton transfer to the catalytic site. The oxidation reaction is linked to proton uptake from solution with time constants coinciding with those of the $P_R \rightarrow F$ and $F \rightarrow O$ transitions and a stoichiometry of 0.7−0.8 H^+ per Cyt*c*O molecule taken up during each transition.[31] Furthermore, changes in the protonation state of a residue, presumably E286, within the D pathway can be indirectly detected by monitoring electron transfer from Cu_A to heme *a* (absorbance changes at 830 nm).[32] In the wild-type Cyt*c*O the electron initially residing at Cu_A equilibrates with heme *a* (~50% oxidation of Cu_A) during the $P_R \rightarrow F$ transition. If this transition is not linked to proton uptake from solution and a negative charge is left behind within

(31) Ädelroth, P.; Ek, M.; Brzezinski, P. *Biochim. Biophys. Acta* **1998**, *1367*, 107.
(32) Karpefors, M.; Ädelroth, P.; Zhen, Y.; Ferguson-Miller, S.; Brzezinski, P. *Proc. Natl. Acad. Sci. U.S.A.* **1998**, *95*, 13606.

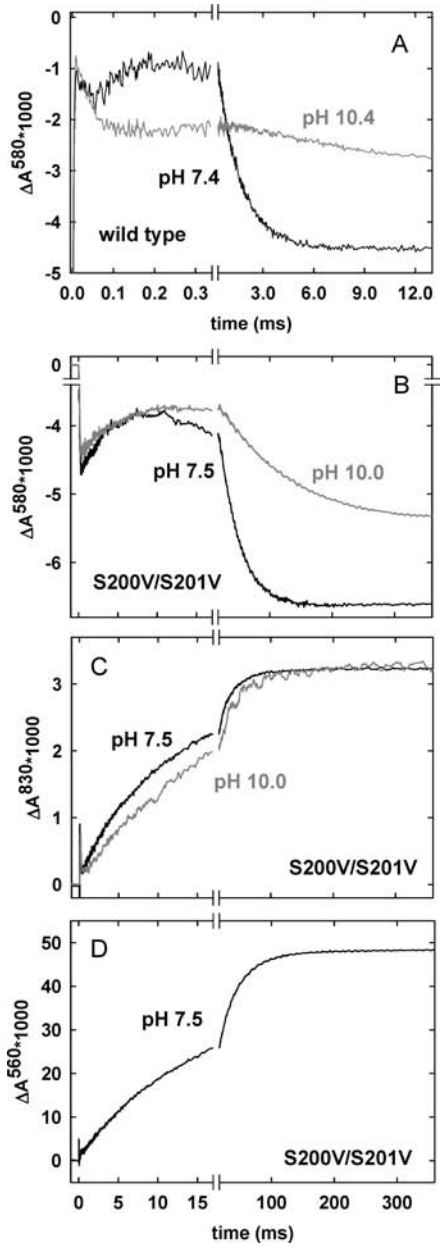

Figure 4. Reaction of the fully reduced Cyt*c*O with O_2. The reaction is initiated at time 0. (A) Reaction of the wild-type Cyt*c*O with O_2 at pH 7.4 and 10.4 at 580 nm. With the pH 7.4 data the increase in absorbance starting around 0.1 ms is associated with the $P_R \rightarrow F$ transition, while the following decrease in absorbance is associated with the $F \rightarrow O$ reaction. At pH 10.4 the $P_R \rightarrow F$ reaction is significantly slower and merges with the $F \rightarrow O$ reaction (only a small net decrease in absorbance is seen). (B) Absorbance changes at 580 nm associated with the reaction of the S200V/S201V double-mutant Cyt*c*O with O_2 at 580 nm at pH 7.5 and 10.0. (C) Absorbance changes at 830 nm associated with the reaction of the S200V/S201V double-mutant Cyt*c*O with O_2 at pH 7.5 and 10.0. The increase in absorbance, associated with the setwise oxidation of Cu_A, occurs concomitantly with the $P_R \rightarrow F$ and $F \rightarrow O$ transitions. (D) Absorbance changes at 560 nm associated with changes in the protonation state of the pH dye phenol red (an increase in absorbance corresponds to proton uptake). The two components correspond to proton uptake during the $P_R \rightarrow F$ (40%) and $F \rightarrow O$ (60%) transitions. Experimental conditions: syringe 1 before mixing, 100 mM HEPES (pH 7.5)/100 mM CAPS (pH 10.0) and 0.05% DDM; 2−3 mM ascorbate; 1−1.5 μM hexaammineruthenium(II) chloride; Cyt*c*O concentration 6−20 μM. In the proton uptake experiment in (D) the buffer was exchanged for the same concentration of KCl, and 100 μM EDTA and 40 μM phenol red were added. The contents of syringe 1 were mixed with an oxygen-saturated solution with the same composition, except no enzyme was present.

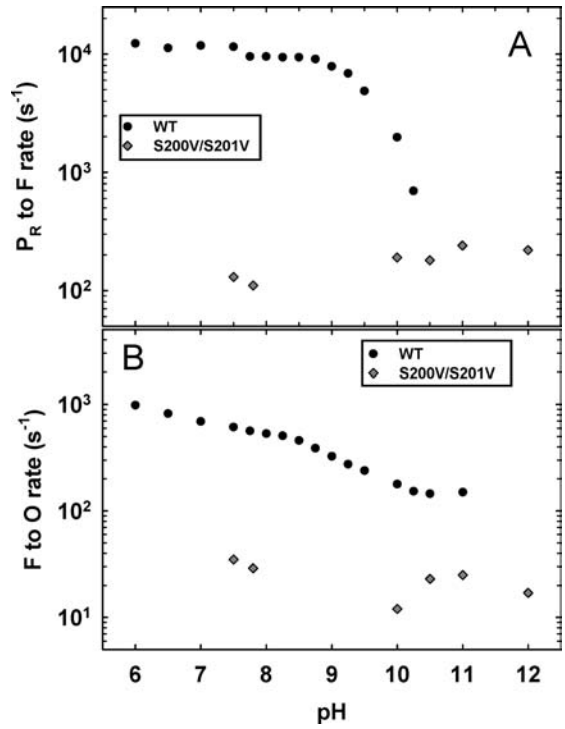

Figure 5. pH dependence of the $P_R \rightarrow F$ (A) and $F \rightarrow O$ (B) transitions. Experimental conditions were the same as in Figure 4, except different buffers were used in different pH ranges (see the Materials and Methods).

the D pathway, this electron transfer does not take place (see the Discussion).

For the S200V/S201V mutant Cyt*c*O, at pH 7.5 the $P_R \rightarrow F$ and $F \rightarrow O$ transitions displayed time constants of 7.7 and 29 ms (Figure 4B), respectively, i.e., slowed by factors of ~70 and ~25, respectively, compared to those of the wild-type Cyt*c*O. As indicated above, the $P_R \rightarrow F$ transition can in principle take place without accompanying proton uptake from solution; the proton needed to form the F state is then transferred internally from the D pathway.[33,34] As seen in Figure 4D, both the $P_R \rightarrow F$ and $F \rightarrow O$ transitions were linked to proton uptake from solution. Furthermore, as in the wild-type Cyt*c*O, the S200V/S201V mutant Cyt*c*O's $P_R \rightarrow F$ transition was linked to electron transfer from Cu_A to heme *a* (Figure 4C; an increase in absorbance at 830 nm indicates oxidation of Cu_A), which also indicates that the reaction does not result in changes in the charge state of the D pathway (i.e., protons are transferred cumulatively all the way from solution to the catalytic site during both the $P_R \rightarrow F$ and $F \rightarrow O$ transitions).

For the S200V/S201Y mutant Cyt*c*O (data not shown) the $P_R \rightarrow F$ and $F \rightarrow O$ transition time constants at pH 7.5 were 14 ms (140 times slower than with the wild-type Cyt*c*O) and 200 ms (200 times slower than with the wild-type Cyt*c*O), respectively. Thus, both transitions were even slower than those in the S200V/S201V mutant.

Figure 5 shows the pH dependence of the $P_R \rightarrow F$ and $F \rightarrow O$ transition rates for the S200V/S201V mutant. The rate of the $P_R \rightarrow F$ transition was essentially pH independent in the range 7.5−12, while the $F \rightarrow O$ transition rate displayed a very small

(33) Smirnova, I. A.; Ädelroth, P.; Gennis, R. B.; Brzezinski, P. *Biochemistry* **1999**, *38*, 6826.
(34) Gorbikova, E. A.; Belevich, N. P.; Wikström, M.; Verkhovsky, M. I. *Biochemistry* **2007**, *46*, 13141.

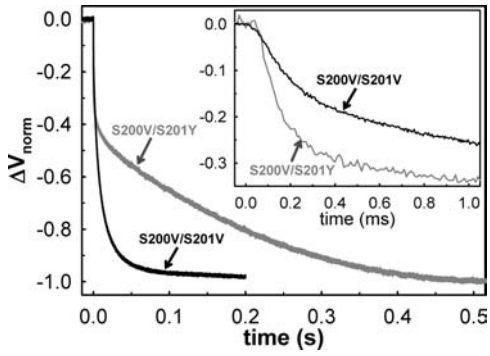

Figure 6. Voltage changes during reaction of the reduced S200V/S201V and S200V/S201Y mutant Cyt*c*O's. The inset shows the first 1 ms of the measurements. Experimental conditions: 50 mM glucose, 0.12 mg/mL glucose oxidase, 75 μg/mL catalase, 50 μM TMPD in a buffer mixture of equal amounts of Bis-Tris propane, CHES, and CAPS (total concentration of 0.1 M, pH 7.5). The CO ligand was dissociated by a laser flash about 0.2 s after injection of 50 μL of an O_2-saturated buffer in a direction toward the Teflon mesh.

pH dependence, decreasing by a factor of ~2 at most upon increasing the pH from 7.5 to 12.

Introduction of the D132N mutation, which blocks proton uptake, into the S200V/S201V mutant resulted in a $P_R \rightarrow F$ time constant of ~5 ms (data not shown), which is very similar to that observed for the S200V/S201V mutation alone. This result is consistent with earlier studies showing that the F state can be formed without proton uptake from solution if the proton needed to form the F state can be taken internally from E286 in the D pathway.[33,34] The next transition, $F \rightarrow O$, was much slower (~0.2 s) in the S200V/S201V/D132N triple mutant than in the S200V/S201V double mutant, which is consistent with earlier results showing that the D132N mutation dramatically slows proton uptake from solution into the D pathway.[33,35]

2.5. Flow-Flash Kinetics: Electrometric Detection. The voltage changes upon oxidation of the fully reduced Cyt*c*O are shown in Figure 6. This is the same reaction as that described above, but in this case the technique is used to detect charge movements within the Cyt*c*O oriented in a membrane.[36] Results from previous studies have shown that in the wild-type Cyt*c*O the voltage changes reflect the $P_R \rightarrow F$ and $F \rightarrow O$ transitions and display time constants of ~100 μs and 0.5−1 ms/1−5 ms (the $F \rightarrow O$ transition is biphasic), respectively.[37] The observed voltage changes are attributed to charge transfer perpendicular to the membrane surface (i.e., transfer of the substrate and pumped protons and electron transfer from Cu_A to heme *a*). In addition, a voltage change that occurs prior to the $P_R \rightarrow F$ transition was recently identified.[38] At neutral pH this voltage change displayed a time constant of ~30 μs in the *Pseudomonas denitrificans* Cyt*c*O (cf. 65 μs with the *R. sphaeroides* Cyt*c*O) and an amplitude that was ~15% of the total voltage change.[38−40] It was attributed to internal proton transfer from E286 to a loading site for pumped protons[38] or charge transfer within the K pathway as a result of electron transfer to the catalytic site.[39]

In the S200V/S201V mutant Cyt*c*O the first component displayed a time constant of ~65 μs (~25% of the total amplitude) and is attributed to the charge transfer discussed above, prior to the $P_R \rightarrow F$ transition. The second and third components displayed time constants similar to those of the $P_R \rightarrow F$ and $F \rightarrow O$ transitions, 6.5 ms (~40% of the total amplitude) and 40 ms (~35% of the total amplitude).

In the S200V/S201Y mutant the first component had a time constant of 65 μs and comprised ~40% of the total amplitude (i.e., a larger fraction than the S200V/S201V mutant). The remaining part of the trace displayed time constants of ~14 ms (~13%) and ~200 ms (47%).

2.6. Preliminary Simulations. To select mutations that were likely to disrupt proton transport through the "trap" region within the D pathway, preliminary MS-EVB2 simulations were run with single and double mutations of the serine residues 200 and 201. These residues were replaced with hydrophobic and polar alternatives, including isoleucine, valine, phenylalanine, and tyrosine. First, the system was prepared from a crystal structure (PDB ID 2GSM) of the oxidized *R. sphaeroides* Cyt*c*O by introducing the oxidized−reduced partial charge distribution,[41] solvating the system in TIP3P water, minimizing, and equilibrating. In each simulation the mutations were introduced with the SwissPDB View Program, selecting the most favorable side chain orientations. Next the system was equilibrated in the absence of the excess proton, and the proton was then introduced just above the N124−N139 bridge and held fixed for 100 ps while the system adjusted to the presence of an extra charge. Following this, the proton was released, and its progress up the pathway was tracked for 1 ns. Systems that blocked the proton below the trap region (see the Introduction) were selected as likely candidates for altered enzyme activity and proton pumping.

2.7. Solvation of the D Pathway from Simulation. To assess the role of solvation in the altered activity and kinetics of the mutated enzymes, the distribution of water molecules in the D pathway was measured both in the presence and in the absence of an excess proton. The distributions for the wild-type and S200V/S201V enzymes (with no excess proton in the pathway) are shown in Figure 7. The integrated values within 3 and 5 Å of E286 are also presented for clarity. A surprising result is that when E286 is protonated (i.e., the state before the $P_R \rightarrow F$ transition), the distributions show that there is not less, as expected, but slightly more water close to E286 in the S200V/S201V mutant. When E286 is deprotonated, however, this trend is switched and E286 is slightly *less* solvated in the mutated enzyme. These subtle differences are consistent with increasing the stability of the protonated form of E286 relative to the deprotonated form and thereby increasing its effective pK_a.

Determining the exact number of water molecules in the D pathway is quite a challenge, as previously demonstrated by Henry et al. for the wild-type enzyme.[1] To ensure our results were not artifacts of having too few or too many waters, the distributions for systems containing 7−13 water molecules were calculated. This is a reasonable range considering the wild-type enzyme was found to have 11−12 waters in the D pathway.[1] As shown in Figure 8A very similar distributions were obtained regardless of the number of waters, suggesting that water molecules sample multiple positions along the pathway when there are too few to fill it completely. The distributions for S200V/S201V with deprotonated E286 are shown in Figure 8A,

(35) Salomonsson, L.; Brändén, G.; Brzezinski, P. *Biochim. Biophys. Acta, Bioenerg.* **2008**, *1777*, 343.
(36) Verkhovsky, M. I.; Morgan, J. E.; Verkhovskaya, M. L.; Wikström, M. *Biochim. Biophys. Acta* **1997**, *1318*, 6.
(37) Jasaitis, A.; Verkhovsky, M. I.; Morgan, J. E.; Verkhovskaya, M. L.; Wikström, M. *Biochemistry* **1999**, *38*, 2697.
(38) Belevich, I.; Verkhovsky, M. I.; Wikström, M. *Nature* **2006**, *440*, 829.
(39) Lepp, H.; Svahn, E.; Faxén, K.; Brzezinski, P. *Biochemistry* **2008**, *47*, 4929.
(40) Lepp, H.; Brzezinski, P. *Biochim. Biophys. Acta. Gen. Subj.* **2009**, *1790*, 552.
(41) Tashiro, M.; Stuchebrukhov, A. A. *J. Phys. Chem. B* **2005**, *109*, 1015.

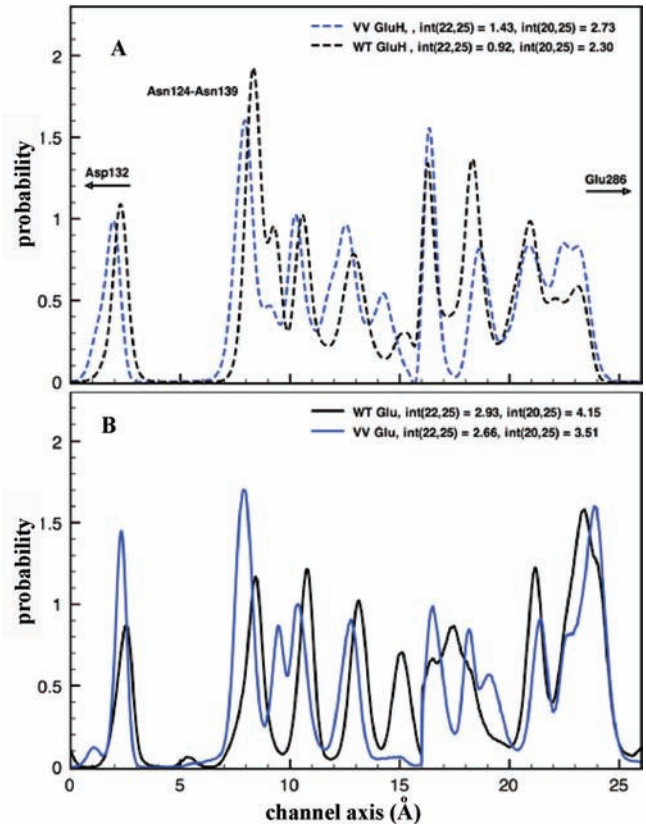

Figure 7. Water distributions along the D pathway for the wild-type and S200V/S01V enzymes. The mean distributions for systems containing 10, 11, and 12 waters are shown when E286 is (A) protonated/neutral and (B) deprotonated/anionic. The integrated water probabilities within 3 and 5 Å of E286 are provided in the legend.

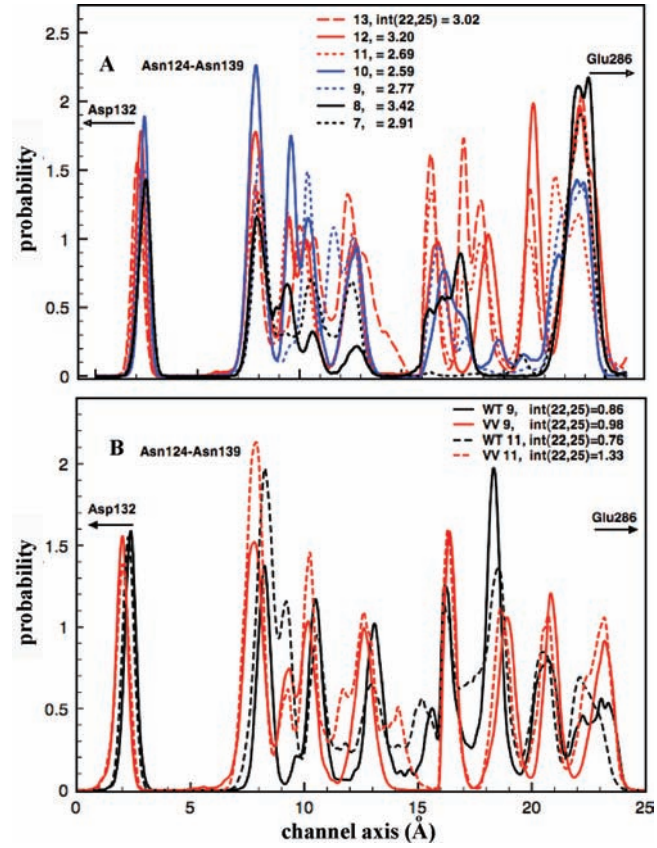

Figure 8. (A) Water distributions for S200V/S201V when E286 is deprotonated and the D pathway contains 7−13 water molecules. (B) Comparison of S200V/S201V distributions to wild-type distributions when E286 is protonated and the D pathway contains 9 and 11 water molecules. Integrated water probabilities within 3 Å are provided in the legend.

but a similar consistency was observed in all of the tested systems. Thus, the trends reported above for the decreased/increased solvation of E286 were consistent for all comparable numbers of waters in the mutated and wild-type enzymes. The results shown in Figure 7, chosen for relevance and clarity, are the average distributions for systems containing 10, 11, and 12 waters. However, even comparing fewer waters (e.g., 9) in S200V/S201V to more (e.g., 11) in the wild-type enzyme (see Figure 8B) generally maintained the same trends. Thus, our findings on altered solvation in the S200V/S201V mutant are not artifacts of the number of water molecules placed in the D pathway.

To estimate the relative proton affinities of E286 in the wild-type and S200V/S201V (VV) enzymes, the average electrostatic potential at the carbonyl oxygen and hydrogen atoms was calculated from simulations with 7−13 water molecules in the D pathway. The results, presented in Table 3, are once again independent of the number of water molecules present in the simulation. When E286 is protonated, the electrostatic potential around the oxygen and hydrogen atoms (OE1 and HE1 in the AMBER force field) is more negative in S200V/S201V than it is in the wild type, suggesting a higher pK_a for S200V/S201V. However, when E286 is deprotonated, the average electrostatic potential around the oxygen atoms (OE1 and OE2) is more negative in the wild-type enzyme, seeming to suggest that S200V/S201V should have a lower pK_a. Thus, the average electrostatic potential only offers a partial explanation for S200V/S201V's shifted pK_a.

Table 3. Electrostatic Potentials for E286

atom	charge[c]	WT	VV	WT	VV	WT − VV
glu OE1[a]	−0.8188	0.461	0.523	−0.358	−0.296	−0.062
glh OE1[b]	−0.5838	0.559	0.526	−0.025	−0.058	0.033
glh HE1[b]	0.4641	−0.581	−0.599	−0.117	−0.135	0.018

[a] Carboxyl oxygen of deprotonated E286. [b] Carboxyl oxygen and hydrogen of protonated E286. [c] Partial charge of the atom in simulations.

2.8. Proton Transport through the D Pathway. When E286 is deprotonated, proton transport from the N124−N139 bridge through the D pathway is a downhill process. This was demonstrated previously for both the wild-type and N98D mutant of bovine Cyt*c*O.[25,27] Figure 9 shows a similar plot for the wild-type and mutated (S200V/S201Y, VY) *R. sphaeroides* enzymes studied herein. The S200V/S201Y mutation was expected to be the most likely to introduce a barrier to proton translocation because (1) it introduces a large barrier in the free energy landscape when E286 is protonated (discussed below), (2) it decreases enzymatic activity substantially (more than S200V/S201V), and (3) it blocks proton pumping completely. Simulations show that the S201Y side chain folds into the pathway, creating steric hindrance and blocking the pathway to E286 when the excess proton is low in the D pathway. As the proton gets closer, however, the tyrosine flips up and out of the way for the proton to proceed toward the negatively charged E286. Although the S200V/S201Y free energy profile is downhill, it is less so than for the wild-type Cyt*c*O and results in a difference of over 17 kcal/mol close to E286. Thus, the mutation is expected to slow proton translocation through this

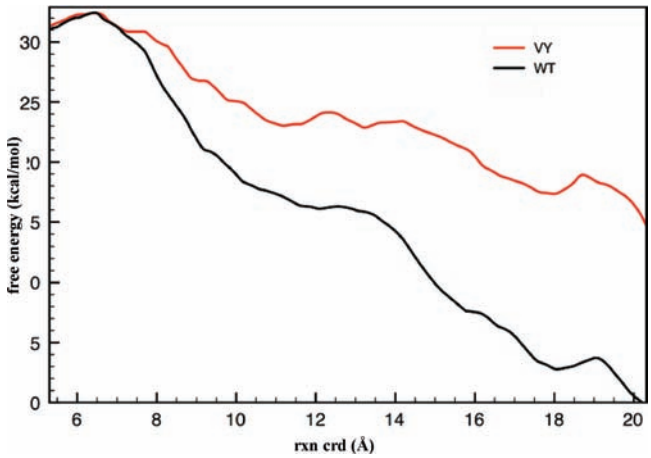

Figure 9. Free energy profile (potential of mean force) for proton transport from the N124−N139 bridge to deprotonated/anionic E286 in the WT and VY enzymes.

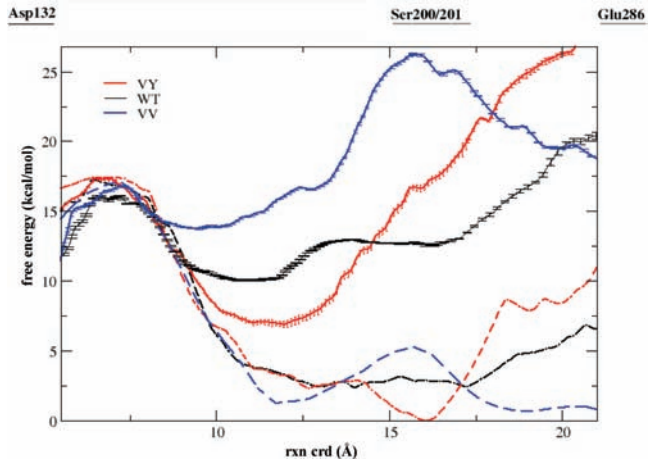

Figure 10. Free energy profiles for proton transport from the N124−N139 bridge to protonated/neutral E286 for the WT, VV, and VY enzymes. Dashed lines represent systems in which water molecules have flooded in and around subunit I. Solid lines (with error bars) represent systems in which no additional water (excluding waters already present in the D pathway and beyond) was allowed to leak beyond the membrane boundary. Error bars on the dashed lines are not shown for clarity, but are comparable to those shown on the solid lines. Similar trends are maintained in both solvation environments.

region of the pathway minimally, but never in a rate-limiting manner that would explain the slowed oxidation kinetics.

This situation is quite different when E286 is protonated. As shown in Figure 10 both the S200V/S201V and S200V/S201Y mutations do significantly change the free energy profiles for proton translocation to the neutral glutamic acid. The stabilization that was previously observed in the bovine Cyt*c*O[25] is less dramatic in the wild-type *R. sphaeroides* Cyt*c*O studied herein. This difference is due to (1) the use of a more realistic solvation and a reaction coordinate that follows the nonlinear D pathway as opposed to following a linear vector, (2) longer sampling times and therefore better convergence in the free energy profiles, and (3) possible differences between the *R. sphaeroides* and bovine enzymes. Figure 10 also shows the same profiles for the wild-type and mutant Cyt*c*O's when water molecules above and below the enzyme have been more tightly controlled and prevented from penetrating around and into subunit (SU) I, as described in the Materials and Methods. These less hydrated profiles show very similar patterns with a higher overall barrier

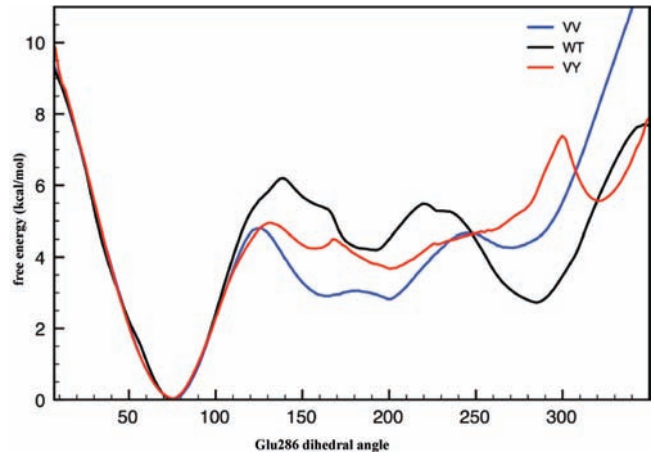

Figure 11. Free energy profile for the rotation of E286 from the down position (∼75°) to the up position (∼290°) for the WT, VV, and VY enzymes.

for proton translocation. The real free energy profiles fall somewhere between these two extremes, when SUs II and III and the surrounding membrane would more accurately screen the electrostatic interactions and desolvation effects. Although these results should not be trusted for quantitative predictions, they do consistently show that proton translocation through the D pathway is hindered (slowed) by the S200V/S201V and S200V/S201Y mutations *when E286 is protonated*.

2.9. E286 Dihedral Rotation. The free energy of rotating the Cα−Cβ−Cγ−Cδ dihedral angle was determined for the wild-type and mutated enzymes, each with E286 protonated. As shown in Figure 11 the barrier for rotation from the "down" position (∼75°) to the "up" (∼290°) position is higher for the wild-type enzyme. The wild-type Cyt*c*O is also, however, more stable once it reaches the up position. Assuming that deprotonation occurs in the up position, the total barrier for proton transfer to the catalytic center would be 1−2 kcal higher in S200V/S201V and S200V/S201Y than in the wild-type Cyt*c*O.

3. Discussion

The D pathway of *R. sphaeroides* aa_3-type Cyt*c*O is used to transfer both protons that are pumped and substrate protons used for reduction of O_2 to water. As described in the Introduction there is a cluster of water molecules ∼7 Å below E286 that is stabilized by hydrogen bonds to residues that line the pathway, including three serines (157, 200, and 201). This water cluster was postulated to play an important role in the proton-pumping mechanism due to the stabilization of an excess proton in this region when E286 is protonated.[25,27,28] One possibility was for this cluster to act as a transient proton donor−acceptor within the pathway, being the primary proton donor to E286 after its deprotonation. In other words, proton transfer was proposed to take place in two steps: deprotonation of E286 and then reprotonation of the glutamic acid from the water cluster followed by immediate proton uptake from solution.

In the present study structural alterations of S200 and S201, predicted from simulation to hinder proton transport, were introduced to challenge the existence of a stable protonated water cluster in the trap region and to further investigate the role of solvation in proton translocation and pumping. The hydrogen bond forming hydroxyl groups in S200 and S201 were replaced with hydrophobic or aromatic and bulky side chains.

3.1. Kinetics and Thermodynamics of Proton Transfer. In all of the structural variants the steady-state activity was lower

than with the wild-type Cyt*c*O. The reduction rates of the S200V/S201V and S200V/S201Y mutant Cyt*c*O's were much less affected than the oxidation rates, which is consistent with previous observations that the K pathway is used for proton transfer during reduction and the D pathway is used during oxidation. Thus, the slowed overall activity was primarily due to slowed oxidation of the enzyme (see Table 2). Replacement of S200 by isoleucine maintained a high activity (~80% of the wild-type activity) and the ability to pump protons. Although the introduction of the bulky isoleucine residue was expected to result in some perturbation of the water cluster coordinated around the S200 and S201 residues, the simulation results show some degree of plasticity in the solvation through this region, while the experimental results show that this degree of plasticity is sufficient for proton pumping. Furthermore, even though removing the hydrogen bonds to the serine residues in the S200V/S201V double mutant Cyt*c*O did affect the proton-pumping stoichiometry (50% of the wild-type value), the ability to pump protons remained in this structural variant. The simulation results show that the water distributions are more altered when E286 is deprotonated, but are not substantially altered in either protonation state. The S200V/S201Y double mutant, on the other hand, displayed a very low activity (11%) and did not pump protons, indicating that this mutation significantly altered the proton pathway. The simulation results, however, show that this alteration does not introduce a barrier to proton transport when E286 is *deprotonated* such that proton transport through the D pathway may be slowed, but not in a rate-limiting manner.

The flow-flash data showed that for both the S200V/S201V and S200V/S201Y mutations proton transfer through the D pathway during the $P_R \rightarrow F$ and $F \rightarrow O$ transitions was significantly slowed. In the S200V/S201V mutant at pH 7.5 the $P_R \rightarrow F$ and $F \rightarrow O$ transitions were slowed by factors of ~70 and ~25, respectively, while in the S200V/S201Y mutant these transitions were slowed by factors of ~140 and ~200, respectively. We note that the $P_R \rightarrow F$ transition at the catalytic site is only associated with proton uptake through the D pathway, while the $F \rightarrow O$ transition also involves simultaneous electron transfer.[42] Because both the proton-transfer rate and the electron equilibrium within Cyt*c*O determine the observed rate of the $F \rightarrow O$ transition, the different effects of the mutations on the $P_R \rightarrow F$ and $F \rightarrow O$ transitions likely reflect (minor) alteration of the electron distribution within the mutant Cyt*c*O.

Upon blocking proton uptake from solution, by introduction of the D132N mutation, in the S200V/S201V mutant Cyt*c*O, the $P_R \rightarrow F$ transition was ~50 times slower than with the wild-type Cyt*c*O; i.e., the transition was slowed by a factor similar to that observed with the S200V/S201V mutation alone. Results from earlier studies have shown that, upon blocking proton uptake from solution with the D132N mutation, the $P_R \rightarrow F$ transition takes place with about the same time constant as that observed with the wild-type Cyt*c*O (~100 μs). Thus, the proton needed at the catalytic site to form the F state must be transferred internally from E286,[33,34] and this proton transfer is the rate-determining step of the $P_R \rightarrow F$ transition.[43] The results from this study show that the same situation is observed with the S200V/S201V mutant Cyt*c*O; the time constants of F formation were ~8 ms without and ~5 ms with the D132N substitution. In other words, the slowed $P_R \rightarrow F$ transition in the S200V/S201V mutant Cyt*c*O must be due to slower proton transfer from E286 to the catalytic site and not due to slowed proton transport through the D pathway. The simulation results show that the mutations only alter proton translocation through the D pathway when E286 is protonated, also supporting the notion that the slowed oxidation kinetics are due to proton transfer from E286 to the catalytic site.

With both the S200V/S201V and S200V/S201Y mutant Cyt*c*O's, voltage changes were observed associated with the $P_R \rightarrow F$ and $F \rightarrow O$ transitions. In addition, a rapid voltage change occurred prior to these transitions with a time constant of ~65 μs. This voltage change was originally attributed to internal proton transfer from E286 to a loading site for pumped protons,[38] but more recent results indicate that it is due to charge transfer within the K pathway as a result of electron transfer to the catalytic site.[39] The relatively larger contribution of this voltage change in the S200V/S201V (~25% of the total amplitude) and S200V/S201Y (~40% of the total amplitude) mutants than in the wild-type Cyt*c*O (~15% of the total amplitude) is consistent with a smaller pumping stoichiometry in the S200V/S201V mutant and lack of proton pumping by the S200V/S201Y mutant. This is assuming that the 65 μs voltage change has essentially unchanged amplitude in these structural variants and that the relative contribution of the remaining voltage changes decreases by 1 unit charge (one instead of two pumped protons) for S200V/S201V and by 2 unit charges (no pumped protons) for S200V/S201Y mutant Cyt*c*O's. Furthermore, the observation that this voltage change displayed essentially the same time constant with the S200V/S201V and S200V/S201Y mutants (where proton transfer from E286 is significantly slowed) as with the wild-type Cyt*c*O is not consistent with the proposal that it is due to proton transfer from E286 (cf. ref 38).

As outlined in the Introduction structural modifications of residues within the D pathway may result in uncoupling of proton pumping from oxygen reduction. Results from studies of these mutant Cyt*c*O's have been important for understanding functional aspects of the proton-pumping machinery. The most clear-cut example of such mutant Cyt*c*O's is the N139D structural variant, which displayed the same (*P. denitrificans* Cyt*c*O[14]) or even higher (*R. sphaeroides* Cyt*c*O[15]) activity as compared to the wild-type Cyt*c*O. In this mutant the proton-transfer rate through the D pathway was unaltered, yet proton pumping was completely impaired. The only detectable alteration was an increase in the E286 pK_a from 9.4 in the wild-type Cyt*c*O[43] to ~11 in the mutant Cyt*c*O.[17] Further replacement of D132 by asparagine in the N139D mutant Cyt*c*O (i.e., N139D/D132N double-mutant Cyt*c*O) resulted in restoration of the proton-pumping activity and a decrease in the E286 pK_a to ~9.7.[21] These results were interpreted to indicate a correlation between a change in the E286 pK_a and a change in the pumping stoichiometry. Furthermore, because in the structural replacements discussed above addition of an extra negative charge (N139D) and removal of another negative charge (N139D/D132N double-mutant Cyt*c*O) correlated with changes in the E286 pK_a, one could speculate that the E286 pK_a changes could be of electrostatic origin. However, the electrostatic effect was found to be a less likely explanation for the altered pK_a on the basis of both theoretical calculations[24] and more recent experimental results (reviewed in ref 11) showing that replacement of N139 by threonine also led to uncoupling of proton pumping from O_2 reduction and a change in the E286 pK_a.[19] However,

(42) Brändén, G.; Brändén, M.; Schmidt, B.; Mills, D. A.; Ferguson-Miller, S.; Brzezinski, P. *Biochemistry* **2005**, *44*, 10466.
(43) Namslauer, A.; Aagaard, A.; Katsonouri, A.; Brzezinski, P. *Biochemsitry* **2003**, *42*, 1488.

in this case the pK_a decreased to ~7.6. These results pointed to a structural alteration as a likely explanation for the altered pK_a and impaired pumping,[22] which is also supported by the recently determined structure of the N139D mutant Cyt*c*O from *P. denitrificans*.[23]

The results for the S200V/S201V mutant reveal another D pathway mutation that alters the E286 pK_a. The $P_R \rightarrow F$ rate was essentially pH independent, while the **F → O** rate displayed only a very weak pH dependence, which indicates that the E286 pK_a increased to a value >12. This larger change in pK_a, as compared to that seen, e.g., with the N139D mutant Cyt*c*O, is consistent with the smaller distance from S200/S201 (6−7 Å) than from N139 (~25 Å) to E286. However, in the case of the S200V/S201V mutant Cyt*c*O the change in the pumping stoichiometry appears not to correlate with the change in the E286 pK_a; despite the larger pK_a shift for the S200V/S201V than for the N139D mutant Cyt*c*O, the former still pumps protons (with a 50% stoichiometry).

3.2. Solvation of the D Pathway from Simulations. The simulation results provide insight into how the mutations alter the solvation in the D pathway and help explain the pK_a shift in S200V/S201V. Given that the serine residues (200 and 201) form strong hydrogen bonds with the water molecules through this region of the pathway, replacing them with valine residues was expected to fill the pathway with bulky hydrophobic side chains, occluding the waters and possibly breaking the hydrogen-bonded chain of waters through the D pathway. This in turn was expected to introduce a barrier to proton transport through this region and to pull waters away from E286, resulting in a more hydrophobic environment. The experimentally determined pK_a increase for E286 in S200V/S201V supported this view since placing E286 in a more hydrophobic environment would destabilize the deprotonated form of the residue (i.e., increase its pK_a).

The simulations revealed just the opposite of what was expected. The valine side chains actually open up more space in the D pathway and increase the solvation around the protonated (neutral) form of E286 (see Figure 7). The negatively charged form of E286 does seem to be less solvated in the presence of the valine mutations, but the difference in both cases is much smaller than expected. These results would indeed cause an up-shifted pK_a in S200V/S201V given that the increased solvation stabilizes the protonated form of E286, which is still a polar residue, while decreased solvation destabilizes the deprotonated form. An increased stability of the protonated form of E286 in S200V/S201V is further supported by the average electrostatic potentials, which are more negative, as well as the free energy profiles for proton transport and side chain rotation, both of which show a lower free energy for the mutated enzyme than for the wild-type Cyt*c*O. Thus, the simulation results show that the cause of this pK_a shift is more subtle (e.g., small changes in solvation) and intricate (e.g., stabilization of the protonated/neutral form of the acid) than expected.

3.3. Importance of Solvation Dynamics during Proton Transport. Multiple crystal structures have captured the presence of (5−10) water molecules in the D pathway. Molecular dynamics simulations have been used to further characterize the solvation environment both through the D pathway (suggesting 11−12 waters) and in the hydrophobic cavity above E286.[1,44−46] Although these findings suggest some of the possible mechanisms of proton transport, they reveal a limited picture of the dynamic solvent environment in the presence of an excess proton. Parts a−d of Figure 12 show the distribution of water molecules through the D pathway both before and during proton migration. The significant alterations in these distributions, also shown in Figure 13, demonstrate how much the excess charge changes both water and protein conformations as it moves. Both water molecules and proximal residues rearrange when the positive excess charge is within interaction range. For example, as soon as the proton dissociates from D132. the oxygen on N124 rotates down toward the excess charge (disrupting the hydrogen bonds between N139 and N124), and the waters above the asparagines move closer to the excess charge and D132. Thus, the distributions and conformations present *before* the proton is released from D132 are very different from those that the proton moves through. Additionally, the diffusions of water molecules into and out of interstitial pockets due to the presence of the excess proton (different from those that would occur before the proton is released from a residue) must also be considered if they occur on time scales that compete with proton translocation through that pocket. In our simulations water molecules occasionally transferred between the hydrophobic region and the D pathway. These findings emphasize that static crystal water wires and MD simulations of solvation environments lacking the excess proton are of limited use in the prediction of proton transport mechanisms.

3.4. Proton Transport Simulations. The simulations show that proton transport through the trap region is a rapid process (downhill free energy profile) in both the wild-type and mutated enzymes when E286 is deprotonated. When E286 is protonated, however, the mutations introduce kinetically significant barriers to proton transport through the trap region. The importance of these results hinges on the question of whether proton transport through the D pathway is ever rate-limiting. If it is, then the simulation results could be explained by a few possibilities. First, the rate-limiting barrier could occur before or after the trap region. Since we are limited to working with a reduced model (SU I only) in the present study, proton transport into the pathway and past the N124−N139 bridge cannot be accurately represented. Therefore, we cannot completely rule out the possibility that the S200V/S201V and S200V/S201Y mutations alter the barrier for proton translocation up to or through the N124−N139 bridge region. This is unlikely because the mutations lie 5−6 Å above the N124−N139 bridge and do not drastically change the solvation around the asparagine bridge, though they do show noticeable changes. Second, we cannot definitively rule out the possibility that the mutants substantially alter the barrier between the ion contact pair (when the proton is immediately below deprotonated E286) and the protonated form of E286. This is also unlikely to be the cause of the slowed oxidation kinetics since the F → O transition should, according to standard transition-state theory, have barriers of ~13.4 and ~15.4 kcal/mol for the wild-type enzyme and S200V/S201V mutant, respectively. The barrier between the ion contact pair and the protonated form of E286 is unlikely to be larger than 5 kcal/mol for any form of the enzyme since this is the value obtained for the protonation of glutamic acid in the bulk phase.[47]

(44) Zheng, X.; Medvedev, D. M.; Swanson, J.; Stuchebrukhov, A. A. *Biochim. Biophys. Acta* **2003**, *1557*, 99.
(45) Olkhova, E.; Michel, H.; Hutter, M. C.; Lill, M. A.; Helms, V. *Biophys. J.* **2004**, 1873.
(46) Seibold, S. A.; Mills, D. A.; Ferguson-Miller, S.; Cukier, R. I. *Biochemistry* **2005**, *44*, 10475.
(47) Maupin, C. M.; Wong, K. F.; Soudackov, A. V.; Kim, S.; Voth, G. A. *J. Phys. Chem. A* **2006**, *110*, 631.

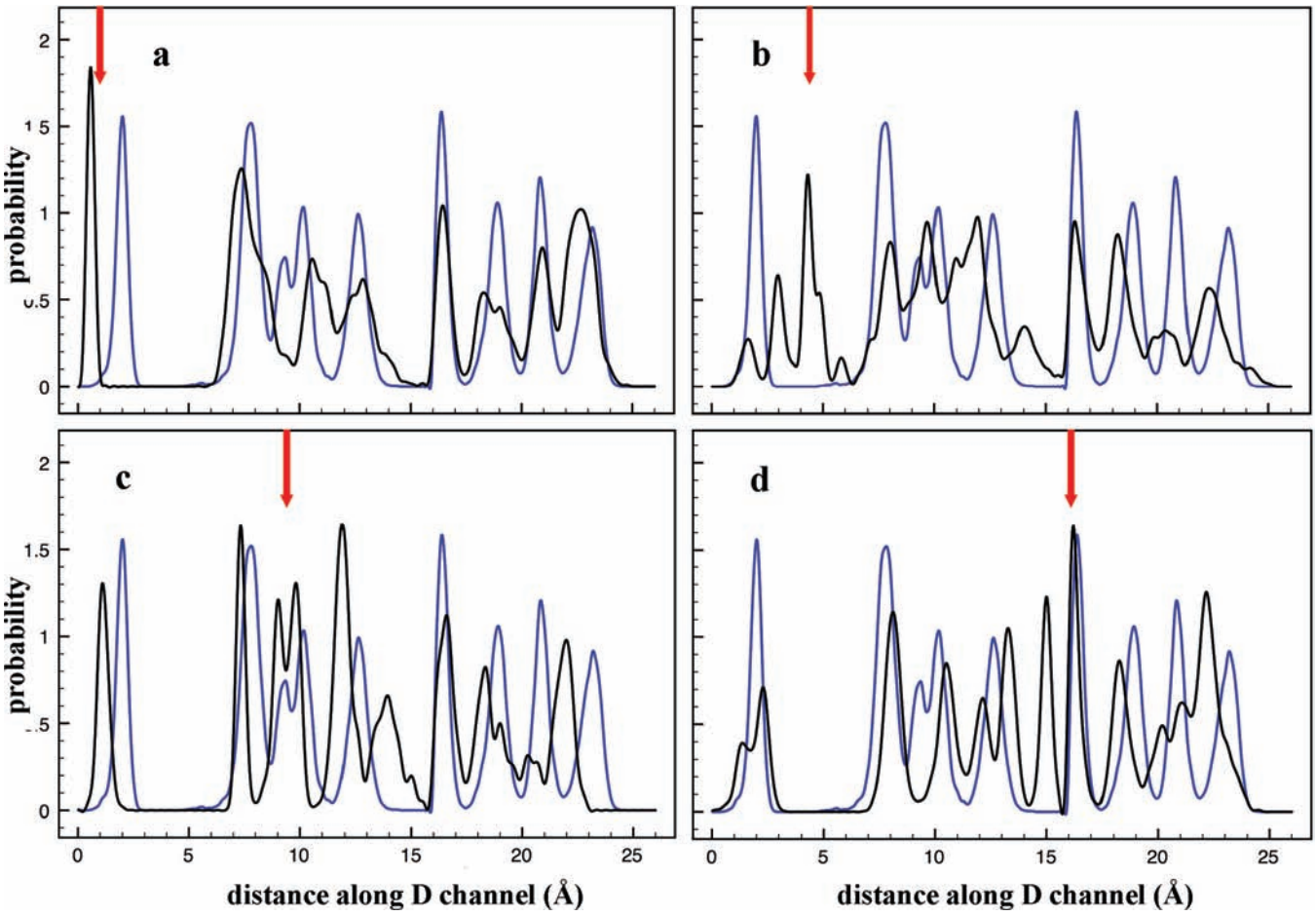

Figure 12. Water distributions for the S200V/S201V enzyme with E286 protonated both with (black) and without (blue) an excess proton migrating through the pathway. The red arrows indicate the position of the excess proton.

Finally, if proton transport through the trap region *is* rate-limiting, then the slowed kinetics in the mutated enzymes could only be attributed to transport to the protonated form of E286. This seems unlikely when one views the proton-pumping mechanism as a series of linked steps since a proton is not thought to transfer through the D pathway until *after* E286 has been deprotonated. In reality, however, this process involves a system in flux, described by a more complex kinetic model in which proton populations transition between intermediates and transient occupancies can influence kinetic outcomes. For example, the deprotonation of E286 is a rare event and is coupled to the deprotonation of D132. As this event occurs there may be transient charge-separated states. The deprotonation of D132 could occur in these periods as well, resulting in a population of protons in the D pathway as E286 is still trying to deprotonate. These protons would of course further facilitate E286 deprotonation (e.g., the P_R to F transition).

This said, the most likely explanation for why the mutated enzymes have slowed oxidation rates but display no barriers to proton transport when E286 is deprotonated is simply that proton transport through the D pathway is not rate-limiting for either the $P_R \rightarrow F$ or the $F \rightarrow O$ transitions. Rather the rate-limiting barrier involves proton transport from E286 to the catalytic site.

3.5. E286 Rotation. It has been previously suggested that the rotation of E286 plays a critical role in unidirectional proton pumping.[48,49] This rotation could be the rate-limiting step, as opposed to or in addition to E286 deprotonation, during the $P_R \rightarrow F$ transition when a proton is transported from E286 to the catalytic site. Therefore, the slowed oxidation rates of the mutants could hypothetically be explained by an increased barrier for dihedral rotation. Similarly, a shift in the stability of the up and down E286 positions could alter the effective pK_a of E286.

Simulation results show that this dihedral rotation is altered by 1−2 kcal/mol in the S200V/S201V mutant. Therefore, the slowed oxidation kinetics, which translates into a ∼2.6 kcal/mol larger barrier for the S200V/S201V mutant, is not accounted for by the rotation alone. The rest of the increased barrier most likely comes from the deprotonation of E286. The average electrostatic potential measured at E286's dissociable proton (more negative for S200V/S201V) further supports this suggestion.

4. Conclusions

The experimental data are summarized in Tables 1 and 2. Theoretical calculations were performed to interpret these results at a molecular level. Together they support the following conclusions.

(48) Kaila, V. R. I.; Verkhovsky, M. I.; Hummer, G.; Wikström, M. *Biochim. Biophys. Acta, Bioenerg.* **2009**, *1787*, 1205.
(49) Kaila, V. R. I.; Verkhovsky, M.; Hummer, G.; Wikström, M. *Biochim. Biophys. Acta, Bioenerg.* **2008**, *1777*, 890.

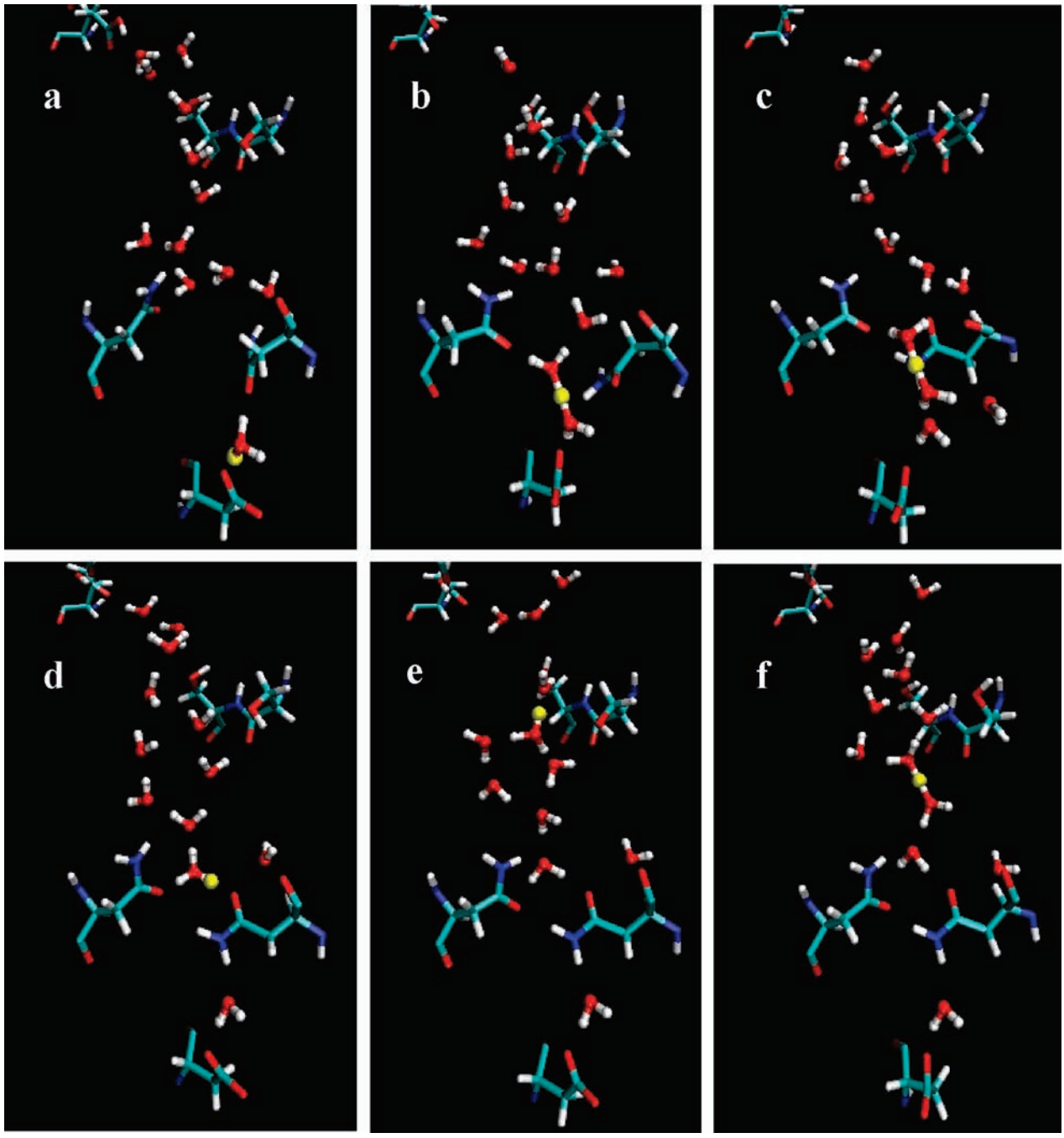

Figure 13. Configurations representative of the water distributions shown in Figure 12, highlighting residues D132 (bottom) and N124, N139, V200, V201, and E286 (top) along with water molecules and the excess proton (yellow).

(1) The mutants alter the solvation in the D pathway, but they do so in an unexpected way. E286 is actually more solvated in the S200V/S201V mutant than it is in wild type when E286 is protonated and less when it is deprotonated. This finding is independent of the number of water molecules (within the tested range of 7−13) in the pathway. These changes must stabilize the protonated form and destabilize the deprotonated form of E286.

(2) The mutants do *not* introduce a barrier to proton transport through the D pathway (from the N124−N139 bridge to E286) when E286 is *deprotonated*. Even for the S200V/S201Y mutant this is a downhill process.

(3) The mutants *do* significantly alter proton transport through the proposed trap region when E286 is *protonated*. The most likely explanation of this is that proton transport through the D pathway is not rate-limiting in either the $P_R \rightarrow F$ or $F \rightarrow O$ transition.

(4) The $P_R \rightarrow F$ transition is not rate-limited by the rotation of E286 from the down to up position. In S200V/S201V, this rotation may be increased by 1−2 kcal, but the rest of the change in the overall barrier must occur during deprotonation. This suggests that the protonated form of E286 in the mutant is more stable than that in the wild type, a notion that is supported by free energy profiles and mean electrostatic potentials.

(5) Results 1 and 4 suggest that the increase in S200V/S201V's pK_a from 9.4 to >12 is caused by a stabilizing increase in solvation around the protonated form of E286 and a destabilizing decrease in solvation around the deprotonated form.

(6) Overall, these simulations show that alterations in the solvent environment have a significant influence on proton transport. These alterations depend on the dynamic response of the water molecules to the presence of the excess proton. The static structure (i.e., water molecules from crystal structures) and dynamic ensembles in the absence of the proton (e.g., from MD simulations) provide a limited picture of the real system and may be misleading when drawing conclusions or predicting proton transport mechanisms.

(7) These simulations were limited to a reduced model of SU I. More conclusive quantitative results will require a full model (SUs I−III) with a multidimensional free energy profile accounting for proton diffusion as well as critical conformational changes (e.g., breaking of the N124−N139 bridge), changes in solvation, and the explicit protonation of E286.

5. Materials and Methods

5.1. Preparation and Characterization of the Mutant Cyt*c*O's. A Quick-Change (Stratagene) mutagenesis kit was used to introduce the mutations. PJS3-SH plasmid[50] was used as a template plasmid, and pRK415-1[51] was used as an expression plasmid for the mutations. The expression plasmid with the mutation was transferred into S-17-1 cells by electroporation, and then the plasmid was transferred into the *R. sphaeroides* JS100 strain by conjugation. The mutations were verified by sequencing (at the UIUC Biotech Center). The His-tagged Cyt*c*O was purified using histidine-affinity chromatography described previously.[50] The Cyt*c*O used for proton-pumping assays was further purified using anion-exchange chromatography (tandem DEAE-5PW column, Toso-HaaS attached to an FPLC system, Amersham, model ÄKTA Basic).

The optical absorption spectra of the oxidized and reduced mutant Cyt*c*O's were the same as those of the wild-type enzyme. The Cyt*c*O concentration was determined from the reduced (red) minus oxidized (ox) absorbance differences (Shimadzu UV/vis-2101PC): A_{605}(red − ox) − A_{630}(red − ox) or A_{606}(red) − A_{640}(red) using an absorption coefficient of 24 or 40 $mM^{-1}cm^{-1}$, respectively.

5.2. Steady-State Activity Measurement. The Cyt*c*O activities were determined by monitoring the oxygen-consumption rates polarographically (YSI model 53 oxygen meter). The reaction chamber contained 1.8 mL of 50 mM potassium phosphate buffer, 0.1% *n*-dodecyl β-D-maltoside (DM) at pH 6.5, 10 mM ascorbate, 0.5 mM TMPD, and 30 μM horse heart cytochrome *c* (Sigma, 96.1% purity).

5.3. Reconstitution of Oxidase into Vesicles and Proton-Pumping Assays. Vesicles containing Cyt*c*O were prepared by mixing 80 mg/mL of soybean IIS lecithin (Fluka), 2% cholic acid, and 100 mM HEPES−KOH at pH 7.4. The mixture was sonicated (model W-375 sonicator, Heat System-Ultrasonics, Inc.) under a stream of argon gas with 1 min sonication and 1.5 min resting cycles until the solution was clear (typically five cycles). Cyt*c*O was added to the vesicle/cholate mixture to a final concentration of 0.9 μM. The detergent was slowly removed by the addition of aliquots of Bio-Beads (66 mg/mL added every 30 min for 4 h at 4 °C). After that Bio-Beads were added at room temperature (133 mg/mL every 30 min for 2 h and, finally, 266 mg/mL every 30 min for 1 h), followed by overnight dialysis in 60 mM KCl.

Proton pumping was measured using a pH electrode as described in ref 16. The stirred cell contained 1.5 mL of 60 mM KCl, 40 μM cytochrome *c*, 10 μM valinomycin, and 0.4 μM Cyt*c*O. Most of the O_2 was removed from this solution by stirring under the stream of water-saturated argon gas. At this point, ascorbate was added to a final concentration of 300 μM. After equilibration, in which the final remnants of O_2 were removed by the oxidase, the reaction was initiated by injection of 10 μL of air-saturated water, equilibrated at 25 °C. A 10 μL volume of 1 mM HCl was then added for calibration. Using the same Cyt*c*O−vesicle preparation, the experiment was repeated in the presence of 10 mM ascorbate. This increases the rate of ascorbate re-reduction of TMPD, releasing one proton/electron. Each of these experiments was repeated again in the presence of protonophore, CCCP (10 μM), to equilibrate the protons on the inside and outside of the vesicles. The proton-pumping stoichiometry (H^+/e^-) was determined by calculating the ratio of the pH changes induced by injection of 10 μL of H_2O to 10 μL of 1 M HCl.

Proton pumping was also measured using a stopped-flow apparatus (Applied Photophysics, SX.17-MV) equipped with a diode-array detector by following changes in the absorbance of the pH dye phenol red at 557 nm (isosbestic point of cytochrome *c* oxidation). The Cyt*c*O−vesicle solution contained 60 mM KCl, 5 μM valinomycin, and 0.4 μM Cyt*c*O at pH 7.4. It was mixed with a solution containing cytochrome *c*, 60 mM KCl, 10 μM reduced cytochrome *c*, and 40 μM phenol red at pH 7.4. The same experiment was repeated with CCCP added to the Cyt*c*O−vesicle solution (see above).

5.4. Stopped-Flow Oxidation and Reduction Kinetics. To determine the oxidation kinetics, 5 μM Cyt*c*O (final concentration) was solubilized in 50 mM Tricine at pH 8.0, 0.1% DM, ~100 μg/mL catalase (from bovine liver, Sigma). The solution was saturated with argon gas, and 400 μM dithionite was added to reduce the enzyme. The reduced Cyt*c*O was mixed with oxygen-saturated 50 mM Tricine pH 8.0 buffer in the stopped-flow apparatus (see above). In this experiment excess dithionite was rapidly oxidized by oxygen, and the reduced Cyt*c*O was oxidized by the excess oxygen.

The reduction kinetics was measured by first oxidizing reduced Cyt*c*O and then following re-reduction as a function of time in a stopped-flow apparatus. Cyt*c*O at a concentration of 5 μM was added to 50 mM Tricine at pH 8.0, and 0.1% DM was loaded into one driving syringe. The buffer containing 10 mM ruthenium(III) hexamine was mixed with 30 mM dithionite and loaded into the other driving syringe. Upon mixing, the reaction of the reduced enzyme with O_2 is rapid, but the excess reductant present then re-reduces the enzyme, which was monitored spectroscopically.

5.5. Flow-Flash Kinetics: Optical Detection. Purified Cyt*c*O at a concentration of 7−20 μM was solubilized in 100 mM HEPES (pH 7.5), 100 mM CAPS (pH 10.0, 10.5, 11.0), or 100 mM potassium phosphate (pH 12) and 0.05% DDM. Complete reduction of the enzyme was obtained by adding 2−3 mM ascorbate and 1−1.5 μM hexaammineruthenium(II) chloride in an anaerobic cuvette under a N_2 atmosphere. After reduction the atmosphere was exchanged for CO, which results in formation of the fully reduced Cyt*c*O−CO complex.

All optical flow-flash measurements were performed using a flow-flash setup described in more detail in ref 52. Briefly, the

(50) Mitchell, D. M.; Gennis, R. B. *FEBS Lett.* **1995**, *368*, 148.
(51) Keen, N. T.; Tamaki, S.; Kobayashi, D.; Trollinger, D. *Gene* **1988**, *70*, 191.
(52) Brändén, M.; Sigurdson, H.; Namslauer, A.; Gennis, R. B.; Ädelroth, P.; Brzezinski, P. *Proc. Natl. Acad. Sci. U.S.A.* **2001**, *98*, 5013.

reduced, CO-bound Cyt*c*O is rapidly mixed (1:5) with an oxygen-saturated buffer (same composition as that in which the enzyme is kept). About 300 ms after mixing the reaction was initiated by removing the blocking CO ligand by a ~10 ns laser flash at 532 nm. The oxidation of Cyt*c*O was monitored by following absorbance changes at various wavelengths (see the figures).

Proton uptake during O_2 reduction was studied as described above, except that unbuffered solutions were used: 100 mM KCl (set to pH 7.8), 0.05% DDM, 100 μM EDTA, and 40 μM phenol red. Changes in phenol red absorbance were monitored at 560 nm.

5.6. Flow-Flash Kinetics: Electrical Detection. Membrane potential generation during reaction of the reduced Cyt*c*O with O_2 was monitored as originally described in ref 36. The setup used in our measurements is described in ref 39. Briefly, a thin Teflon film, separating two compartments, was soaked in lipids (100 mg of soybean IIS lecithin/mL of *n*-decane). Liposome-reconstituted Cyt*c*O was fused to the surface by incubation in 0.1 M MOPS, pH 7.5, and 12 mM $CaCl_2$. Subsequently, the compartments where carefully washed to remove the liposomes that had not fused to the measuring membrane. The solution was replaced by a mixture of equal amounts of Bis-Tris propane, CAPS, and CHES buffer (total concentration 0.1 M, pH 7.5), and Ag/AgCl electrodes (DRIREF-2SH, World Precision Instruments) were inserted on each side of the measuring membrane. After the atmosphere was changed, first to N_2 and then to CO, 50 mM glucose, 0.12 mg/mL glucose oxidase, 75 μg/mL catalase, and 50 μM *N*,*N*,*N*′,*N*′-tetramethyl-*p*-phenylenediamine (TMPD) were added to both compartments. The reaction was initiated by flashing off the CO ligand bound to the catalytic site of Cyt*c*O, using a laser, 0.2 s after injection of 50 μL of O_2-saturated buffer in the direction toward the measuring membrane.

5.7. Simulation Setup and Procedure. The system was prepared from a 2.0 Å resolution crystal structure (PDB ID 2GSM) of the oxidized *R. sphaeroides* enzyme. Consistent with previous simulations,[25,27,28] a reduced model composed of subunit I, internal water molecules, and a layer of water molecules above and below the protein was used in the present study. The partial charges of heme a_3 and Cu_B were adjusted to reflect the reduced catalytic site.[41] Depending on the simulation at hand, water molecules were either added to or removed from the D channel and the hydrophobic region above E286. The excess proton was added at the channel entrance, and counter charges were placed in the bulk solvent region for charge neutrality. To maintain structural integrity, all Cα atoms greater than 5 Å from the D channel were tethered to their crystal structure positions with a loose ($k = 1$) harmonic potential.

The water distributions of 7−13 water molecules were calculated with 200 ps of equilibration followed by 2−5 ns of sampling. The simulations were run with a 1 fs time step in the NVT ensemble (300 K) with the Nose−Hoover thermostat and a relaxation constant of 0.2 ps. Electrostatic interactions were calculated with the smooth particle mesh Ewald summation using a tolerance of 10^{-5} and real-space cutoff of 11 Å. The same cutoff was applied to Lennard-Jones interactions. Each system was run in duplicate starting from different initial water positions. In this case, D132 was protonated and E286 was either protonated or deprotonated.

Initially the water molecules above and below the protein were allowed to penetrate into membrane-like regions around the protein. This was effectively stabilizing water higher in the D pathway and providing additional pathways for water penetration and escape. Adding a membrane-like boundary to the system (hydrophobic spheres along the membrane surface) eliminated this spurious oversolvation and resulted in quite different free energy profiles for proton transport through the D pathway.

The MS-EVB method, a substantial extension of the original two-state EVB approach,[53] used to describe proton transport and solvation in condensed-phase and biomolecular systems, has been extensively described elsewhere.[54−58] Briefly, this approach defines the excess proton (a charge defect) as a linear combination of empirically motivated valence bond "states" $|i\rangle$, each of which localizes the proton on a different water molecule. A Hamiltonian is defined with the potential energy for independent states in diagonal elements and the coupling between states in off-diagonal elements:

$$H^{\mathrm{EVB}}(\vec{r}) = \sum_{ij} |i\rangle h_{ij}(\vec{r}) \langle j|$$

where $\vec{r}$ is the complete set of nuclear coordinates. Diagonalizing this matrix at each time step generates a reactive potential energy surface along which the nuclei can be evolved with Newton's equations of motion. The eigenvector with the smallest eigenvalue (lowest energy) contains the coefficients c_i for each state's contribution to the ground-state (reactive) potential energy surface. The protein interactions are herein represented by the AMBER99 force field,[59] the water is represented by a flexible TIP3P model,[56] and the excess proton is represented by the second-generation MS-EVB parameter set.[56]

Explicit proton transfer between water and amino acids, such as E286, was not explicitly allowed in the present study. To identify and track the location of the excess proton, which is delocalized over many water molecules, a new coordinate called the center of excess charge (CEC) is defined:

$$X_{\mathrm{CEC}} = \sum_{i=1}^{N_{\mathrm{EVB}}} c_i^2 x_i$$

in which c_i is the coefficient (weighting) of each state and x_i is the location of that state's hydronium ion. The MS-EVB2 simulations were carried out with the DL_POLY package[60] modified to include the MS-EVB2 algorithm. Depending on the simulation, E286 and D132 were either protonated or deprotonated while the rest of the residues remained in their default protonation states.

5.8. Free Energy Profiles. The free energy profiles of proton transport through the D pathway were calculated with 12−30 umbrella sampling windows in which the CEC was forced, via harmonic restraint, to sample a given section of the D pathway. Restraining the projection of the CEC onto two vectors provided a more revealing reaction coordinate than the single-vector *z*

(53) Warshel, A.; Weiss, R. M. *J. Am. Chem. Soc.* **1980**, *102*, 6218.
(54) Swanson, J. M. J.; Maupin, C. M.; Chen, H.; Petersen, M. K.; Xu, J.; Wu, Y.; Voth, G. A. *J. Phys. Chem. B* **2007**, *111*, 4300.
(55) Voth, G. A. *Acc. Chem. Res.* **2006**, *39*, 143.
(56) Day, T. J. F.; Soudackov, A. V.; Åœuma, M.; Schmitt, U. W.; Voth, G. A. *J. Chem. Phys.* **2002**, *117*, 5839.
(57) Schmitt, U. W.; Voth, G. A. *J. Chem. Phys.* **1999**, *111*, 9361.
(58) Schmitt, U. W.; Voth, G. A. *J. Phys. Chem. B* **1998**, *102*, 5547.
(59) Wang, J.; Cieplak, P.; Kollman, P. A. *J. Comput. Chem.* **2000**, *21*, 1049.
(60) Smith, W.; Forester, T. R. *CCLRC*; Daresbury Laboratory: Daresbury, Warrington, England, 1999.

coordinate used in previous studies. The relative free energy along the pathway was then calculated with the weighted histogram analysis method (WHAM).[6162] Each window was equilibrated in the constant NVT ensemble for 200 ps followed by 1−1.5 ns of data collection. Umbrella force constants ranging from 20 to 90 kcal mol^{-1} $Å^{-2}$ were used to ensure sufficient overlap between neighboring windows.

A similar process was carried out for the rotation of E286. An umbrella restraint was applied to the $C\alpha-C\beta-C\gamma-C\delta\mu$ dihedral angle, showing its down to up rotation. Multiple solvation environments were tested by increasing and decreasing the number of waters above and below E286. The general trend, as expected, was that solvation stabilized the protonated side chain, but barring extreme desolvation, the reported trends between the wild-type and mutant enzymes were consistent.

Acknowledgment. The experimental part of this study was supported by grants from the NIH and the Swedish Research Council. J.M.J.S. was funded by the Division of Chemical Sciences, Geosciences and Biosciences, Office of Basic Energy Sciences, U.S. Department of Energy, through Grant DE-FG02-09ER16055. G.A.V. was funded by the National Institutes of Health (Grants R01-GM53148 and R01-GM25154).

JA107244G

(61) Kumar, S.; Bouzida, D.; Swendsen, R. H.; Kollman, P. A.; Rosenberg, J. M. *J. Comput. Chem.* **1992**, *13*, 1011.
(62) Roux, B. *Comput. Phys. Commun.* **1995**, *91*, 275.